

Absolute forbidden bands and waveguiding in two-dimensional phononic crystal plates

J. O. Vasseur,^{1,*} P. A. Deymier,² B. Djafari-Rouhani,¹ Y. Pennec,¹ and A-C. Hladky-Hennion¹

¹Institut d'Electronique, de Micro-électronique et de Nanotechnologie, UMR CNRS 8520, Cité Scientifique, 59652 Villeneuve d'Ascq Cedex, France

²Department of Materials Science and Engineering, University of Arizona, Tucson, Arizona 85721, USA

(Received 27 September 2006; revised manuscript received 11 December 2007; published 12 February 2008)

We introduce a supercell plane wave expansion (SC-PWE) method for the calculation of elastic band structures of two-dimensional phononic crystal plates. We compute the band structure of solid-solid and air-solid two-dimensional phononic crystal plates. The air is modeled as a low impedance medium (LIM) with very low density and very high velocities of sound. We investigate the influence of the constituent materials, of the plate thickness, and of the geometry of the array on the band structure. We establish the range of validity of the SC-PWE method in terms of the rate of convergence with respect to the number of plane waves and contrast in physical properties of the matrix and inclusion materials. We show that for high contrast solid-solid phononic crystal plates, our SC-PWE method, as other PWE-based methods introduced to date, suffers from convergence difficulties. In the case of air (modeled as the LIM) holes-solid plates, we demonstrate that the SC-PWE method leads to fast convergence for a wide range of values of solid physical properties. With these constituent materials, we find that the largest absolute forbidden bands occur in the band structure of the phononic crystal plate provided the thickness of the plate is of the order of magnitude of the periodicity of the array of inclusions. We demonstrate the existence of guided modes in an air-silicon phononic crystal plate containing a linear defect.

DOI: 10.1103/PhysRevB.77.085415

PACS number(s): 43.20.+g, 43.40.+s, 63.20.-e

I. INTRODUCTION

Phononic crystals, also named acoustic band gap (ABG) materials are composite materials made of two- or three-dimensional periodic distributions of inclusions embedded in a matrix. The periodic structure of these composite materials gives them peculiar properties, in particular, the existence, under certain conditions, of absolute acoustic band gaps, i.e., forbidden bands that are independent of the direction of propagation of the incident elastic wave.^{1–4} Absolute band gaps confer to these artificial materials' potential applications as sound insulators or for the filtering and demultiplexing of acoustic waves.^{5,6}

Earlier studies of bulk phononic crystals, i.e., phononic crystals assumed of infinite extent along the three spatial directions, have shown that the bandwidth of the forbidden band depends strongly on the contrast between the physical characteristics (density and elastic moduli) of the inclusions and the matrix, as well as the geometry of the array of inclusions, the inclusion shape, and the filling factor of inclusions.^{1–4} More recently, various authors have studied theoretically the existence of surface acoustic waves (SAWs) localized at the free surface of a semi-infinite two-dimensional (2D) phononic crystal.^{7–10} For this geometry, the parallel inclusions are of cylindrical shape and the surface considered is perpendicular to their axis. Various arrays of inclusions,^{7,8} crystallographic symmetries of the component materials,⁹ and also the piezoelectricity of one of the constituent¹⁰ were taken into account. In these studies, the same method of computation of the SAW band structure was applied. This method is based on the well-known plane wave expansion (PWE) method^{1–4} with SAW explicitly searched as solutions of the Fourier-transformed equation of propagation, exponentially decreasing along the cylinder direction and by im-

posing the proper boundary conditions on the free surface. This method initially developed by Tanaka and Tamura⁷ for semi-infinite 2D phononic crystals exhibiting a single free surface was applied to compute the band structures of 2D phononic crystal plates, with two free surfaces.^{11,12} For example, the symmetric Lamb mode band structures of 2D phononic crystal plates composed of triangular arrays of W cylinders in a Si background were calculated.¹¹ More recently, Charles *et al.*¹² reported on the band structure of a slab made of a square array of Fe cylinders embedded in a Cu matrix. Nevertheless, no absolute stop bands were reported in these studies. Hsu and Wu¹³ combined Mindlin's plate theory and the plane wave expansion method for the calculation of the lower dispersion curves in the band structure of 2D gold-epoxy phononic crystal plates. While accurate, this method, however, is restricted to thin plates. Moreover, Manzanares-Martinez and Ramos-Mendieta have also considered the propagation of acoustic waves along a surface parallel to the cylinders in a 2D phononic crystal.¹⁴ R. Sainidou and Stefanou investigated with the help of the layer-multiple scattering method, the guided elastic waves in a glass plate coated on one side with a periodic monolayer of polymer spheres immersed in water.¹⁵ On the experimental point of view, Wu *et al.*¹⁶ observed high frequency SAW with a pair of interdigital transducers placed on both sides of a very thick silicon plate in which a square array of holes was drilled. Similar experiments were conducted by Benchabane *et al.* on a 2D square lattice piezoelectric phononic crystal etched in lithium niobate.¹⁷ Zhang *et al.*¹⁸ have shown the existence of gaps for acoustic waves propagating at the surface of an air-aluminum 2D phononic crystal plate through laser ultrasonic measurements.

In this paper, we use a supercell PWE (SC-PWE) method to calculate the band structure of a 2D phononic crystal plate of finite thickness along the axis of the cylinders. We high-

light the differences between 2D bulk phononic crystal dispersion curves and the band structure of the phononic crystal plate. We investigate the influence of the constituent materials, and of the plate thickness, and of the geometry of the array on the band structure. Furthermore we identify the conditions for convergence of the SC-PWE method in terms of the contrast in the physical properties of the constitutive materials of the phononic crystal plate. We focus on 2D phononic crystal plates made of solid cylindrical inclusions embedded in a solid material and on arrays of air holes drilled in a solid matrix. In the case of air holes-solid matrix phononic crystal plates, we characterize the optimum conditions for the existence of wide absolute forbidden bands upon variations of the thickness of the plate. Finally, we demonstrate that removing cylinders in a phononic crystal plate with a forbidden band to form a waveguide leads to the existence of guided acoustic modes.

This paper is organized as follows. In Sec. II, we present the model and, with some details, the method of calculation of the acoustic band structure of 2D phononic crystal plates. Several numerical results are then presented in Sec. III concerning solid-solid and air-solid 2D phononic crystal plates. Section IV contains a discussion of these results and the main conclusions drawn from this study.

II. MODELS AND METHODS OF CALCULATION

A. Plane wave expansion method for bulk phononic crystals

We first briefly recall the basic principles of the PWE method used for the calculation of the band structures of bulk 2D phononic crystals. These composite materials are modeled as periodic arrays of infinite cylinders of different shapes (circular, square, etc.) made up of a material *A* embedded in an infinite matrix *B*. Elastic materials *A* and *B* may be isotropic or of specific crystallographic symmetry. The elastic cylinders are assumed parallel to the *z* axis of the Cartesian coordinates system (*O*, *x*, *y*, *z*). The intersections of the cylinders axis with the (*xOy*) transverse plane form a 2D periodic array and the nearest neighbor distance between cylinders is *a*. The 2D primitive unit cell may contain one cylinder or more. The filling factor, *f_i*, of each inclusion is defined as the ratio between the cross-sectional area of a cylinder and the surface of the primitive unit cell.

In absence of an external force, the equation of propagation of the elastic waves in any composite material is given as:

$$\rho(\vec{r}) \frac{\partial^2 u_i(\vec{r}, t)}{\partial t^2} = \sum_{j,m,n} \frac{\partial}{\partial x_j} \left[C_{ijmn}(\vec{r}) \frac{\partial u_n(\vec{r}, t)}{\partial x_m} \right], \quad (1)$$

where *u_i(r̂, t)* is a component (*i*=*x*, *y*, *z*) of the elastic displacement field. The elements *C_{ijmn}* (*i*, *j*, *m*, *n*=1, ..., 6) of the elastic stiffness tensor and the mass density *ρ* are periodic functions of the position vector, *r̂*=(*r̂_{||}*, *z*)=(*x*, *y*, *z*). In the particular case of bulk phononic crystals, i.e., assumed of infinite extent along the three spatial directions *x*, *y*, and *z*, the elastic constants and the mass density do *not* depend on *z*. Then taking advantage of the 2D periodicity in the (*xOy*) plane, they can be expanded in Fourier series in the form

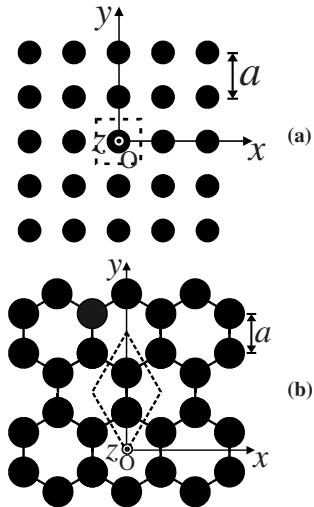


FIG. 1. Transverse cross section of the square (a) and of the graphite (b) arrays. The cylinders are parallel to the *z* direction. The dotted lines represent the primitive unit cell of the 2D array.

$$C_{ijmn}(\vec{G}_{||}) = \sum_{\vec{G}_{||}} C_{ijmn}(\vec{G}_{||}) e^{i\vec{G}_{||}\cdot\vec{r}_{||}}, \quad (2)$$

$$\rho(\vec{r}_{||}) = \sum_{\vec{G}_{||}} \rho(\vec{G}_{||}) e^{i\vec{G}_{||}\cdot\vec{r}_{||}}, \quad (3)$$

where $\vec{G}_{||}=(G_x, G_y)$ is a 2D reciprocal-lattice vector. One writes, with the help of the Bloch theorem, the elastic displacement field as

$$\vec{u}(\vec{r}) = e^{i(\omega t - \vec{K}_{||}\cdot\vec{r}_{||} - K_z z)} \sum_{\vec{G}_{||}} \vec{u}_K(\vec{G}_{||}) e^{i\vec{G}_{||}\cdot\vec{r}_{||}}, \quad (4)$$

where $\vec{K}=(\vec{K}_{||}, K_z)=(K_x, K_y, K_z)$ is a wave vector and ω an angular frequency. If one assumes that $K_z=0$ then the vibrations in the (*xOy*) plane (called XY or mixed-polarization modes) decouple from those parallel to the *z* direction denoted *Z* modes (transverse modes).^{1,4} Substituting Eqs. (2)–(4) into Eq. (1) leads to a standard eigenvalue equation for which the size of the matrices involved depends on the number of 2D $\vec{G}_{||}$ vectors taken into account in the Fourier series. The numerical resolution of the eigenvalue equation is performed along the principal directions of propagation of the 2D irreducible Brillouin zone of the array of inclusions.

In this paper, phononic crystals with square lattice and graphite array are considered (see Fig. 1). For a square lattice of inclusions [see Fig. 1(a)], with one cylinder of filling factor *f* located at the center of the 2D primitive unit cell, the Fourier coefficients in Eqs. (2) and (3) are given as

$$\begin{aligned} \zeta(\vec{G}_{||}) &= \frac{1}{A_u} \int \int_{\substack{(\text{primitive}) \\ (\text{unit cell})}} \zeta(\vec{r}_{||}) e^{-i\vec{G}_{||}\cdot\vec{r}_{||}} d^2\vec{r}_{||} \\ &= \begin{cases} f\zeta_A + (1-f)\zeta_B & \text{if } \vec{G}_{||} = \vec{0} \\ (\zeta_A - \zeta_B)F(\vec{G}_{||}) & \text{if } \vec{G}_{||} \neq \vec{0} \end{cases} \end{aligned} \quad (5)$$

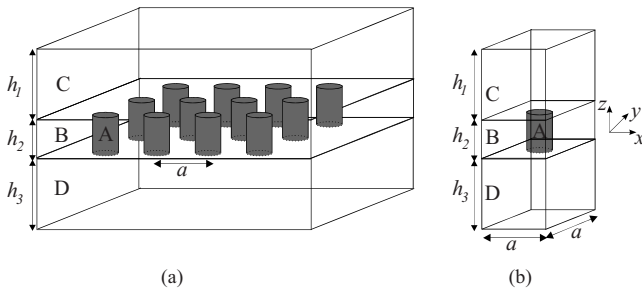


FIG. 2. (a) 2D phononic crystal plate sandwiched between two slabs of homogeneous materials, and (b) three-dimensional supercell considered in the course of the SC-PWE computation.

where $\zeta \equiv \rho$, C_{ijmn} , and A_u is the area of the 2D primitive unit cell. $F(\vec{G}_{||})$ is the structure factor defined as

$$F(\vec{G}_{||}) = \frac{1}{A_u} \int \int_{(A)} e^{-i\vec{G}_{||}\vec{r}} d^2\vec{r}_{||}. \quad (6)$$

In Eq. (6), the integral is performed over the cross section of the inclusion. For cylinders of circular cross section of radius R , the structure factor is

$$F(\vec{G}_{||}) = 2f \frac{J_1(G_{||}R)}{G_{||}R}, \quad (7)$$

where J_1 is the Bessel function of the first kind, $f = \pi R^2 / a^2$ and $0 \leq f \leq \pi/4$. The components of the 2D reciprocal lattice vectors $\vec{G}_{||}$ are $G_x = \frac{2\pi}{a} n_x$ and $G_y = \frac{2\pi}{a} n_y$, where n_x and n_y are integers. In the course of the numerical calculations, we consider $-M_x \leq n_x \leq +M_x$ and $-M_y \leq n_y \leq +M_y$ (with M_x and M_y positive integers), i.e., that $(2M_x+1)(2M_y+1)$ 2D $\vec{G}_{||}$ vectors [G_x and G_y have $(2M_x+1)$ and $(2M_y+1)$ different values, respectively] are taken into account. This gives $3(2M_x+1)(2M_y+1)$ eigenfrequencies ω for a given wave vector \vec{K} . In the graphite network [see Fig. 1(b)], the inclusions are located at the vertices of a regular hexagon and the distance between two nearest neighbors is a . The 2D primitive unit cell with a lozenge pattern of side $a\sqrt{3}$ contains two identical cylinders of filling factors f_1 and f_2 , located at \vec{r}_i ($i=1, 2$) and the Fourier coefficients become

$$\zeta(\vec{G}_{||}) = \begin{cases} f\zeta_A + (1-f)\zeta_B & \text{if } \vec{G}_{||} = \vec{0} \\ (\zeta_A - \zeta_B)F(\vec{G}_{||}) \left(\frac{e^{-i\vec{G}_{||}\vec{r}_1} + e^{-i\vec{G}_{||}\vec{r}_2}}{2} \right) & \text{if } \vec{G}_{||} \neq \vec{0}, \end{cases} \quad (8)$$

where $F(\vec{G}_{||})$ has the same meaning as above; $f=f_1+f_2$ is the total filling factor of inclusion with $f_1=f_2=2\pi R^2/3\sqrt{3}a^2$ ($0 \leq f_1, f_2 \leq \pi/6\sqrt{3}$) for cylindrical inclusions. The components of the 2D reciprocal lattice vectors $\vec{G}_{||}$ are $G_x = \frac{2\pi}{a\sqrt{3}}(n_x - n_y)$ and $G_y = \frac{2\pi}{a\sqrt{3}}\left(\frac{n_x+n_y}{\sqrt{3}}\right)$, where n_x and n_y are integers.⁴

B. Plane wave expansion method for phononic crystal plates

To calculate the elastic band structures of 2D phononic crystal plates, one modifies the PWE method presented above. The phononic crystal plate of thickness, h_2 , is assumed infinite in the (xOy) plane of the Cartesian coordinates system (O, x, y, z). The plate is sandwiched between two slabs of thicknesses h_1 and h_3 , made of elastic homogeneous materials C and D [see Fig. 2(a)]. In the course of the numerical calculations, one considers the parallelepipedic supercell depicted in Fig. 2(b). The basis of the supercell in the (xOy) plane includes that of the 2D primitive unit cell (which may contain one cylinder or more) of the array of inclusions and its height along the z direction is $\ell = h_1 + h_2 + h_3$. This supercell is repeated periodically along the x , y , and z directions. This triple periodicity allows one to develop the elastic constants and the mass density of the constituent materials as Fourier series as

$$\zeta(\vec{r}) = \sum_{\vec{G}} \zeta(\vec{G}) e^{i\vec{G} \cdot \vec{r}}, \quad (9)$$

where $\vec{r} = (\vec{r}_{||}, z) = (x, y, z)$ and $\vec{G} = (\vec{G}_{||}, G_z) = (G_x, G_y, G_z)$ are *three-dimensional position vectors and reciprocal lattice vectors*, respectively. Moreover the elastic displacement field can be written as

$$\vec{u}(\vec{r}) = e^{i(\omega t - \vec{K}_{||} \cdot \vec{r}_{||} - K_z z)} \sum_{\vec{G}} \vec{u}_{\vec{K}}(\vec{G}) e^{i\vec{G} \cdot \vec{r}}. \quad (10)$$

The components in the (xOy) plane of the \vec{G} vectors depend on the geometry of the array of inclusions (see Sec. II A) while along the z direction, $G_z = \frac{2\pi}{\ell} n_z$ where n_z is an integer. The Fourier coefficients in Eq. (10) are now given as

$$\zeta(\vec{G}) = \frac{1}{V_u} \int \int \int_{(\text{super cell})} \zeta(\vec{r}) e^{-i\vec{G} \cdot \vec{r}} d^3\vec{r}, \quad (11)$$

with $V_u = A_u \cdot \ell$ is the volume of the supercell.

For a square array of inclusions, the Fourier coefficients become

$$\zeta(\vec{G}) = \begin{cases} f\zeta_A\left(\frac{h_2}{\ell}\right) + (1-f)\zeta_B\left(\frac{h_2}{\ell}\right) + \zeta_C\left(\frac{h_1}{\ell}\right) + \zeta_D\left(\frac{h_3}{\ell}\right) & \text{if } \vec{G} = \vec{0} \\ (\zeta_A - \zeta_B)F_I^s(\vec{G}) + (\zeta_C - \zeta_B)F_{II}^s(\vec{G}) + (\zeta_D - \zeta_B)F_{III}^s(\vec{G}) & \text{if } \vec{G} \neq \vec{0}, \end{cases} \quad (12)$$

with

$$F_I^s(\vec{G}) = \frac{1}{V_u} \int \int \int_{(A)} e^{-i\vec{G} \cdot \vec{r}} d^3 \vec{r} = F(\vec{G}_{||}) \begin{bmatrix} \sin\left(G_z \frac{h_2}{2}\right) \\ \left(G_z \frac{h_2}{2}\right) \end{bmatrix} \left(\frac{h_2}{\ell}\right), \quad (13a)$$

$$F_{II}^s(\vec{G}) = \frac{1}{V_u} \int \int \int_{(C)} e^{-i\vec{G} \cdot \vec{r}} d^3 \vec{r} = \begin{bmatrix} \sin\left(G_x \frac{a}{2}\right) \\ \left(G_x \frac{a}{2}\right) \end{bmatrix} \begin{bmatrix} \sin\left(G_y \frac{a}{2}\right) \\ \left(G_y \frac{a}{2}\right) \end{bmatrix} \times \begin{bmatrix} \sin\left(G_z \frac{h_1}{2}\right) \\ \left(G_z \frac{h_1}{2}\right) \end{bmatrix} \left(\frac{h_1}{\ell}\right) e^{-iG_z[(h_1+h_2)/2]}, \quad (13b)$$

$$F_{III}^s(\vec{G}) = \frac{1}{V_u} \int \int \int_{(D)} e^{-i\vec{G} \cdot \vec{r}} d^3 \vec{r} = \begin{bmatrix} \sin\left(G_x \frac{a}{2}\right) \\ \left(G_x \frac{a}{2}\right) \end{bmatrix} \times \begin{bmatrix} \sin\left(G_y \frac{a}{2}\right) \\ \left(G_y \frac{a}{2}\right) \end{bmatrix} \begin{bmatrix} \sin\left(G_z \frac{h_3}{2}\right) \\ \left(G_z \frac{h_3}{2}\right) \end{bmatrix} \left(\frac{h_3}{\ell}\right) e^{-iG_z[(h_2+h_3)/2]}. \quad (13c)$$

In Eqs. (13a)–(13c), the integration is performed over the volume occupied by each material A, C, or D inside the unit cell. In Eq. (13a), $F(\vec{G}_{||})$ is the structure factor defined by Eq. (7) for cylindrical inclusions.

For the graphite network, the Fourier coefficients become

$$\zeta(\vec{G}) = \begin{cases} f\zeta_A\left(\frac{h_2}{\ell}\right) + (1-f)\zeta_B\left(\frac{h_2}{\ell}\right) + \zeta_C\left(\frac{h_1}{\ell}\right) + \zeta_D\left(\frac{h_3}{\ell}\right) & \text{if } \vec{G}_{||} = \vec{0} \\ (\zeta_A - \zeta_B)F_I^g(\vec{G}) \left(\frac{e^{-i\vec{G}_{||} \cdot \vec{\tau}_1} + e^{-i\vec{G}_{||} \cdot \vec{\tau}_2}}{2} \right) + (\zeta_C - \zeta_B)F_{II}^g(\vec{G}) + (\zeta_D - \zeta_B)F_{III}^g(\vec{G}) & \text{if } \vec{G} \neq \vec{0}, \end{cases} \quad (14)$$

with

$$F_I^g(\vec{G}) = \frac{1}{V_u} \int \int \int_{(A)} e^{-i\vec{G} \cdot \vec{r}} d^3 \vec{r} = F(\vec{G}_{||}) \begin{bmatrix} \sin\left(G_z \frac{h_2}{2}\right) \\ \left(G_z \frac{h_2}{2}\right) \end{bmatrix} \left(\frac{h_2}{\ell}\right), \quad (15a)$$

$$F_{II}^g(\vec{G}) = \frac{1}{V_u} \int \int \int_{(C)} e^{-i\vec{G} \cdot \vec{r}} d^3 \vec{r} = \begin{bmatrix} \sin\left(G'_x \frac{a\sqrt{3}}{2}\right) \\ \left(G'_x \frac{a\sqrt{3}}{2}\right) \end{bmatrix} \begin{bmatrix} \sin\left(G'_y \frac{a\sqrt{3}}{2}\right) \\ \left(G'_y \frac{a\sqrt{3}}{2}\right) \end{bmatrix} \begin{bmatrix} \sin\left(G_z \frac{h_1}{2}\right) \\ \left(G_z \frac{h_1}{2}\right) \end{bmatrix} \times \left(\frac{h_1}{\ell}\right) e^{-iG_z[(h_1+h_2)/2]}, \quad (15b)$$

$$F_{III}^g(\vec{G}) = \frac{1}{V_u} \int \int \int_{(D)} e^{-i\vec{G} \cdot \vec{r}} d^3 \vec{r} = \begin{bmatrix} \sin\left(G'_x \frac{a\sqrt{3}}{2}\right) \\ \left(G'_x \frac{a\sqrt{3}}{2}\right) \end{bmatrix} \begin{bmatrix} \sin\left(G'_y \frac{a\sqrt{3}}{2}\right) \\ \left(G'_y \frac{a\sqrt{3}}{2}\right) \end{bmatrix} \begin{bmatrix} \sin\left(G_z \frac{h_3}{2}\right) \\ \left(G_z \frac{h_3}{2}\right) \end{bmatrix} \times \left(\frac{h_3}{\ell}\right) e^{-iG_z[(h_2+h_3)/2]}, \quad (15c)$$

where

$$G'_x = \frac{G_x + \sqrt{3}G_y}{2}, \quad G'_y = \frac{-G_x + \sqrt{3}G_y}{2}. \quad (16)$$

As for the bulk phononic crystals, the equation of motion is Fourier transformed by substituting Eqs. (9) and (10) in Eq. (1) and one has again to resolve a standard eigenvalue equa-

tion. The numerical resolution of this eigenvalue equation is performed along the principal directions of propagation of the 2D irreducible Brillouin zone of the array of inclusions while K_z is fixed to any value lower than $\frac{\pi}{\ell}$. In the course of the numerical calculations, G_x , G_y , and G_z take, respectively, $(2M_x+1)$, $(2M_y+1)$, and $(2M_z+1)$ discrete values and this leads to $3(2M_x+1)(2M_y+1)(2M_z+1)$ eigenfrequencies for a given wave vector \vec{K} .

The supercell method requires an interaction as low as possible between the vibrational modes of neighboring periodically repeated phononic crystal plates. Then, in order to allow the top surface of the plate to be free of stress, medium C should behave, for instance, like vacuum.¹⁴ However, as already observed by various authors,^{14,19,20} the choice of the physical parameters characterizing vacuum in the course of the PWE computations is of critical importance. Indeed, in the framework of the PWE method, taking abruptly $C_{ijmn}=0$ and $\rho=0$ for vacuum leads to numerical instabilities and unphysical results.^{14,19,20} Then vacuum must be modeled as a pseudosolid material with very low C_{ijmn} and ρ . For the sake of simplicity, this low impedance medium (LIM) is supposed elastically isotropic and is characterized by a longitudinal speed of sound C_ℓ , and a transversal speed of sound C_t or equivalently by two elastic moduli expressed with the Voigt notation as $C_{11}=\rho C_\ell^2$ and $C_{44}=\rho C_t^2$. The choice of the values of these parameters is governed by the boundary condition between any solid material and vacuum. Indeed, one knows that this interface must be free of stress and this requires that $C_{11}=0$ and $C_{44}=0$ rigorously in vacuum.^{10,14} Then, using the LIM to model vacuum in the PWE computations, the nonvanishing values of these parameters must be as small as possible and we consider that the ratio between the elastic moduli of the LIM and those of any other solid material constituting the phononic crystal must approach zero. We choose C_ℓ and C_t to be much larger than the speeds of sound in usual solid materials in order to limit propagation of acoustic waves to the solid. Large speeds of sound and small elastic moduli impose a choice of a very low mass density for the LIM. More specifically, we choose $\rho=10^{-4}$ kg m⁻³ and $C_\ell=C_t=10^5$ m s⁻¹, i.e., the acoustic impedances of the LIM are equal to 10 kg m⁻² s⁻¹. With these values $C_{11}=C_{44}=10^6$ N m⁻² and the elastic constants of the LIM are approximately 10^4 times lower than those of any usual solid material that are typically on the order of 10^{10} N m⁻². The values we choose for C_{11} and C_{44} are a compromise to achieve satisfactory convergence of the SC-PWE method and still satisfy boundary conditions. Values of the elastic constants of the LIM lower than 10^4 N m⁻² can have, in some cases, effects on the numerical convergence. We choose $C_{11}=C_{44}$ for convenience. In the course of the PWE calculations, these values of the LIM physical characteristics allow one to model vacuum without numerical difficulties. One can also note that our choice of unphysical high speeds of sound for the LIM such as $\frac{1}{C_\ell^2}=\frac{1}{C_t^2}\rightarrow 0$ is consistent with the numerical condition $\frac{\rho_{air}}{C_{ijmn}^{air}}\rightarrow 0$, derived by Tanaka *et al.* for computing accurately the PWE bulk band structures of air-solid 2D phononic crystals.²⁰

In the supercell, medium D can be either vacuum or a homogeneous material depending on whether one wants to

TABLE I. Mass density ρ and elastic constants C_{11} , C_{12} , and C_{44} of Fe, Cu, steel, epoxy, and Si.

Material	ρ (kg m ⁻³)	C_{11} (10^{10} N m ⁻²)	C_{12} (10^{10} N m ⁻²)	C_{44} (10^{10} N m ⁻²)
Fe (cubic)	7867	22.6	14.0	11.6
Cu (cubic)	8932	16.83	12.21	7.57
Steel (isotropic)	7780	26.4		8.1
Epoxy (isotropic)	1142	0.754		0.148
Si (cubic)	2331	16.578	6.394	7.962

model a phononic crystal plate or a structure made of a phononic crystal plate deposited on a substrate of finite thickness. Throughout the present paper, we restrict ourselves to isotropic materials A , B , and D or to constituents of cubic crystallographic symmetry. Finally, with our numerical method, computations of dispersion curves of phononic crystal plates with $K_z=0$ and with any other nonvanishing value of K_z , lower than $\frac{\pi}{\ell}$, lead to nearly the same result. Indeed the eigenvalues computed with $K_z=0$ and $K_z\neq 0$ differ only in their third decimal. This indicates that the homogeneous slabs C and D made of the LIM modeling vacuum rigorously provide appropriate decoupling of the plate modes of vibration in the z direction. Then, throughout this paper, the value of K_z has been fixed to zero.

III. NUMERICAL RESULTS

A. Solid-solid 2D phononic crystal plates

1. Low contrast solid-solid systems

We first apply our SC-PWE method to the calculation of the band structure of a phononic crystal plate made of a square array (lattice parameter a) of iron cylinders, and of circular cross section of radius R , embedded in a copper background. Fe and Cu are materials of cubic crystallographic symmetry and their physical properties (density and elastic constants) present a low contrast¹² (see Table I). The filling factor ($f=\pi R^2/a^2$) and the thickness of the plate are $f=0.564$ and $h_2=0.7a$, respectively. Figure 3(a) shows the band structure of the bulk phononic crystal (hollow squares) and of the phononic crystal plate (black filled dots). The band structure of the bulk phononic crystal was computed with the classical PWE method (see Sec. II A). Applying the SC-PWE method, one obtains the dispersion curves of the plate. In this case, materials C and D are made of LIM and the thicknesses h_1 and h_3 were chosen equal to a . 169 and 343 (i.e., $M_x=M_y=6$ and $M_x=M_y=M_z=3$) reciprocal lattice vectors were taken into account for the computations of the band structures of the bulk phononic crystal and of the phononic crystal plate, respectively. One observes the characteristic nearly parabolic shape in the vicinity of the Γ point of the antisymmetric Lamb mode A_0 . This is the slowest of the modes starting at the Γ point. In this particular structure, the symmetric Lamb mode S_0 and the first transverse mode

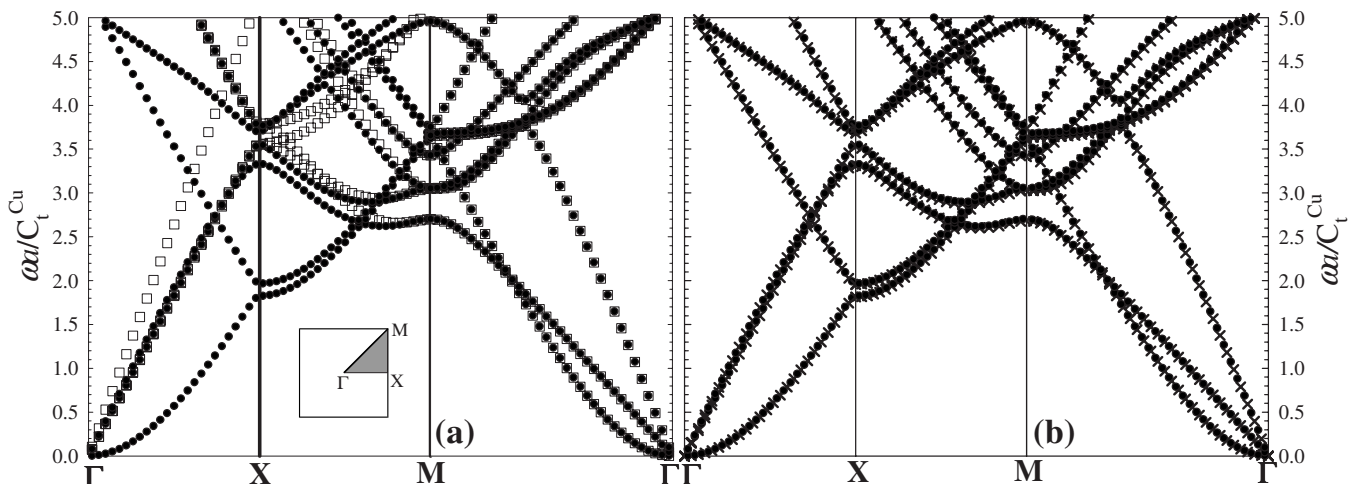


FIG. 3. (a) PWE elastic band structures for the bulk 2D phononic crystal (open squares) and the phononic crystal plate of thickness $h_2=0.7a$ (black filled circles) made of a square array of Fe cylinders of cylindrical cross section embedded in a Cu background with $f=0.564, 169$, and 343 (i.e., $M_x=M_y=6$ and $M_x=M_y=M_z=3$) reciprocal lattice vectors were taken into account for the computations of the PWE band structures of the bulk phononic crystal and of the phononic crystal plate, respectively. The inset represents the first Brillouin zone ($\Gamma X M$) of the square array. The components of the wave vector \vec{K} at the Γ , X , and M points are $\frac{2\pi}{a}(0,0)$, $\frac{2\pi}{a}(\frac{1}{2},0)$, and $\frac{2\pi}{a}(\frac{1}{2},\frac{1}{2})$. A dimensionless frequency $\omega a/C_t^{\text{Cu}}$, where C_t^{Cu} is the transverse speed of sound in Cu, is reported on the vertical axis. (b) SC-PWE (black filled dots) and FEM (black crosses) band structures of the same plate. Note the excellent agreement between the band structures of the plate derived from the two methods of calculation.

nearly overlap. These band structures are nearly the same as those published in Ref. 12. In this reference, the dispersion curves of the plate were derived with the help of the PWE method, by imposing the stress free boundary conditions on the top and bottom surfaces of the plate.¹² However, this latter method requires sampling of both wave vector and frequency while the SC-PWE method generates the eigenvalues (frequencies) by sampling only over the wave vector. In the case of the Fe/Cu system, the SC-PWE method achieves satisfactory convergence at a lower computational cost than the PWE method with stress free surface boundary conditions. Slight differences occur between the values of the eigenfrequencies computed with our SC-PWE method and those obtained by Charles *et al.*, especially for modes of higher order. This can be attributed to a better convergence of our method due to the larger number of reciprocal lattice vectors taken into account (343 compared to 25). Moreover, Fig. 3(a) does not exhibit some pseudomodes without physical meaning which can occur when solving the Fourier transform of the equations of propagation with stress free boundary conditions at the surfaces.^{7,8} One notes also that due to the very low contrast between the elastic constants and density of Fe and Cu, these band structures do not exhibit absolute band gap. To verify the validity of the application of the SC-PWE method to low contrast solid-solid systems, we have also calculated the band structure of the same plate using the finite element method (FEM).²¹⁻²³ In all FEM calculations reported in this paper, we have ensured that the FEM mesh is fine enough for complete convergence of the FEM band structure. These FEM band structures are subsequently used as reference for characterizing the rate of convergence of the SC-PWE method. The SC-PWE (black filled dots) and FEM (black crosses) plate band structures are plotted in Fig. 3(b). One observes the excellent agreement be-

tween the results derived from the two calculation methods. This indicates the very good convergence of our SC-PWE method for low contrast solid-solid 2D phononic crystal plates with a reasonably small number of plane waves (i.e., 343) taken into account. The calculations reported in Fig. 3(b) were done with $h_1=h_3=a$. We have verified the agreement between the SC-PWE and the FEM band structures for h_1 and h_3 varying from $0.5a$ to $1.5a$. This range of thickness for media C and D effectively forbid the interaction between the vibrational modes of neighboring periodically repeated phononic crystal plates. Subsequently we fixed $h_1=h_3=a$ throughout the paper. Finally, we also checked that our SC-PWE method leads to similar results to those published by Tanaka and Tamura⁷ for another low contrast solid-solid system, namely, a 2D semi-infinite phononic crystal composed of a square array of AlAs cylinders in a GaAs matrix. For this, we increased the thickness of the plate to a value of three times the lattice parameter and verified that the zero order symmetric and antisymmetric plate modes fuse into the Rayleigh wave propagating at the free surface of a 2D semi-infinite phononic crystal. Our SC-PWE band structure includes additional bands that arise from the finite thickness of the plate. As the thickness increases further the number of extra bands increases. However, due to the limited number of reciprocal vectors that can be taken into account, the convergence of the numerical calculations fails when considering a very large thickness of the plate.²⁴

2. High contrast solid-solid systems

Here we consider the case of 2D phononic crystal plates made of arrays of steel inclusions embedded in epoxy resin. These solids possess very different densities and elastic constants and the bulk phononic crystal exhibits very large absolute band gaps provided the filling factor of inclusion is

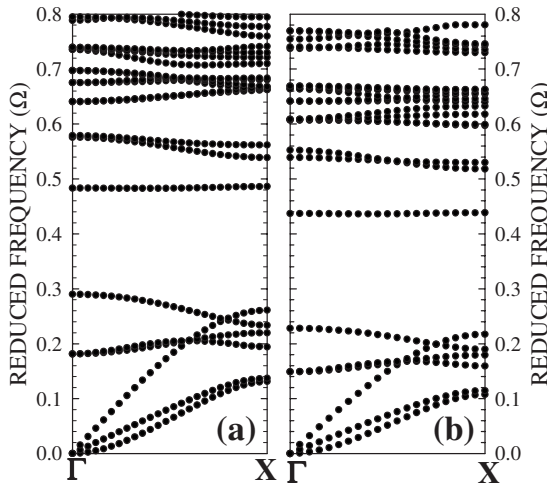


FIG. 4. Band structures along the Γ X direction of propagation of a 2D phononic crystal plate composed of a square array of steel cylinders embedded in an epoxy matrix calculated with (a) the SC-PWE method and (b) the FE method. The SC-PWE calculation used $M_x=M_y=6$, $M_z=2$, i.e., 845 plane waves. The filling factor of inclusions and the thickness of the plate are $f=0.564$ and $h_2=a$.

sufficiently large.⁴ Steel and epoxy resin are isotropic materials and their physical characteristics are reported in Table I.²⁵

Figure 4(a) shows the SC-PWE band structure in the Γ X direction of propagation, of a phononic crystal plate composed of inclusions of circular cross section placed on a square array with thickness $h_2=a$. The filling factor f ($=\pi R^2/a^2$) is equal to 0.564. The results are rendered in terms of a reduced frequency $\Omega=\omega a/2\pi\bar{C}_t$, versus a reduced wave vector $\vec{k}=\vec{K}a/2\pi$ where $\bar{C}_t=\sqrt{C_{44}/\rho}=\sqrt{C_{44}(\vec{G}=0)/\rho(\vec{G}=0)}$ is an average transverse speed of sound. Here the calculation is done with $M_x=M_y=6$, $M_z=2$. For comparison, the FEM band structure of the same plate is reported in Fig. 4(b). Although the shape of the dispersion curves is quite similar in the SC-PWE and FE calculations, the values of the eigenfrequencies differ significantly by about 15%. This result suggests that the SC-PWE method with $M_x=M_y=6$, $M_z=2$ has not converged for the high con-

trast solid-solid phononic crystal plate. In Fig. 5, we analyze the convergence of the SC-PWE method at the X point of the square Brillouin zone for a steel-epoxy phononic crystal plate of thickness $h_2=a$ and $f=0.564$ by varying M_x , M_y , and M_z , i.e., the number of plane waves. On one hand, for this relatively small thickness of the plate, the SC-PWE eigenfrequencies appear to be significantly less sensitive to the choice of M_z than $M_x=M_y$. On the other hand, comparison with the FE method shows that even with 1575 plane waves (i.e., $M_x=M_y=8$, $M_z=2$) the frequencies have not converged and remain about 10% above the FEM results. Note that this pathological lack of convergence for high contrast solid-solid systems is also observed in the PWE method with stress free boundary conditions.^{12,13} This problem also arises in the calculation of the band structure of bulk high contrast 2D phononic crystals.¹⁻⁴ For example, in steel-epoxy bulk 2D phononic crystals, the PWE eigenvalues start to converge satisfactorily for $M_x=M_y=12$. It seems that all the PWE-based methods introduced to date for computing the band structures of high contrast solid-solid 2D phononic crystal plates suffer from convergence difficulties and do not constitute a reliable numerical tool in this case.^{13,24}

B. Air-solid 2D phononic crystals

Since in all band structures reported previously the reduced frequency Ω scales as the inverse of the lattice parameter of the array of inclusions, a , the domain of frequency where forbidden band gaps may occur also scales as $1/a$. The design of phononic crystal plates with forbidden gaps in the mega- or gigahertz range requires periodicity of the array of inclusions of the order of the micro- or the nanometer. From an experimental point of view, the realization at this scale of 2D phononic crystals constituted of two different solid materials is a very challenging task while actual techniques based, for example, on reactive ion etching (RIE), focused ion beam (FIB), or interference lithography allows one to drill relatively easily regular network of holes in a solid.^{10,26} Consequently, with the aim of designing structures exhibiting absolute band gaps at very high frequencies that can be fabricated experimentally, we focus our attention on arrays of holes drilled in a solid matrix. We consider two types of matrix materials, namely, steel and silicon.

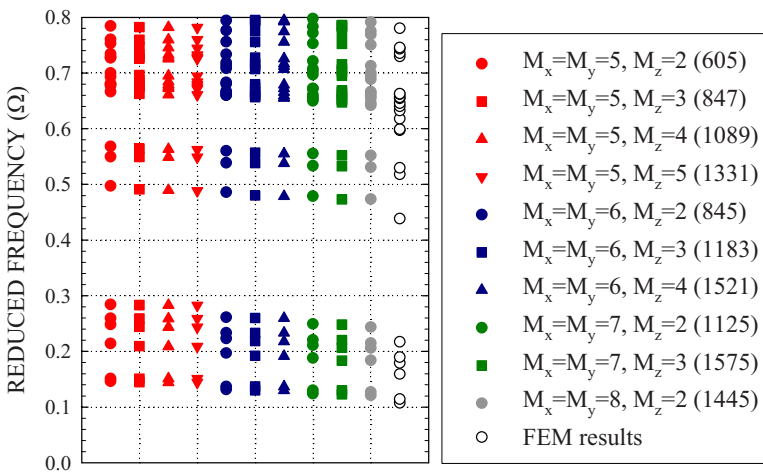


FIG. 5. (Color online) Eigenvalues at the X point of the Brillouin zone calculated with the SC-PWE method as a function of M_x , M_y , and M_z (i.e., the number of plane waves) for the steel-epoxy phononic crystal plate of Fig. 4. The open circles represent the eigenvalues computed with the FE method and serve as a fully converged reference. The integer $N=(2M_x+1)(2M_y+1)(2M_z+1)$ in parentheses indicates the number of plane waves taken into account in the SC-PWE calculations. The standard eigenvalue equation to be resolved involves square matrices of size equals to $3N \times 3N$. Note the poor convergence of the SC-PWE method and the relative insensitivity to M_z for our relatively thin plate.

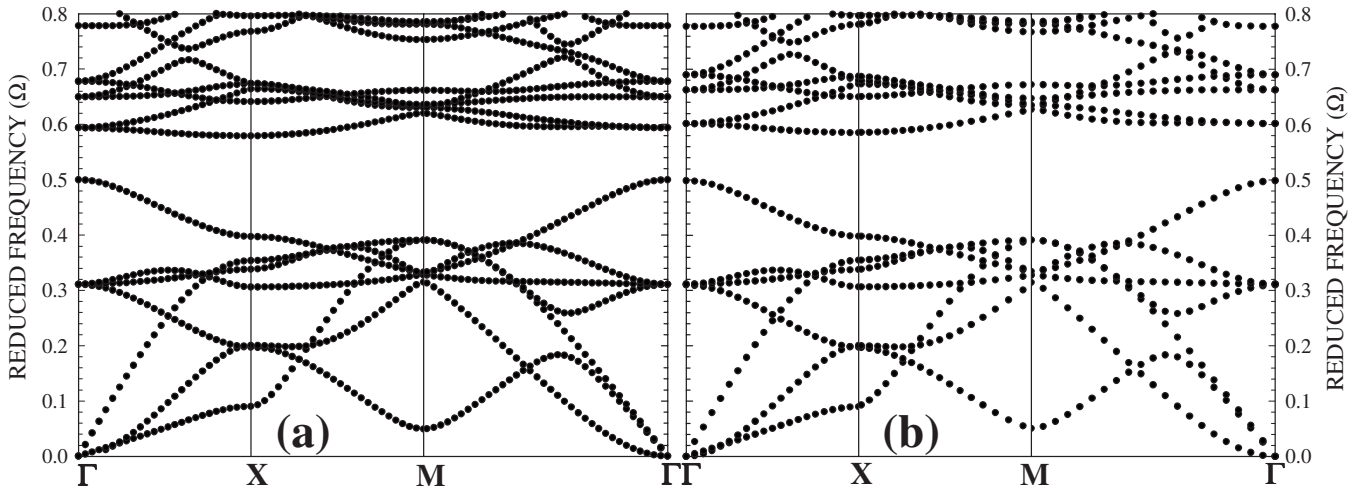


FIG. 6. Band structure of a 2D phononic crystal plate composed of a square array of holes drilled in a steel plate calculated with (a) the SC-PWE method and (b) the FE method. The SC-PWE calculation used $M_x=M_y=4$, $M_z=2$, i.e., 405 plane waves and the air holes were modeled with the LIM. The filling factor of inclusions and the thickness of the plate are $f=0.7$ and $h_2=a$. Note the excellent agreement between the eigenvalues of the two band structures.

1. Air-isotropic matrix systems

Figure 6 shows the elastic band structure of a phononic crystal plate made of a square array of cylindrical holes in steel calculated with the SC-PWE method with $M_x=M_y=4$, $M_z=2$ and the FE method. With these constituent materials, the choice of the filling factor is of particular importance. Indeed, most of the theoretical and experimental studies conducted on bulk 2D phononic crystals have shown that larger gaps are obtained when the inclusions are made of the stiffer material.^{1,4} Nevertheless, a very compact array of holes, for example, a square array of holes drilled in a solid with a filling factor near the closed packed value (i.e., $f=\pi/4$ or $R/a=0.5$), can be visualized as a square array of singular shape solid inclusions embedded in air. Consequently one may expect large gaps for high filling factor of holes.²⁷ This is indeed observed in Fig. 6 where $f=0.7$, i.e., $R/a=0.472$. In the course of the SC-PWE numerical calculations, the material inside the holes, i.e., air, was modeled by the LIM depicted in Sec. II B. With these very large contrast material

constituents the SC-PWE band structure has converged to the FEM results with 405 plane waves. It is worth noting that the air inclusions are not included in the FEM mesh and their effect is accounted for through stress free boundary conditions at the surface of the holes. We further analyze the rate of convergence of the SC-PWE method as a function of the number of plane waves taken into account in the Fourier series expansion in Fig. 7 at the X point of the Brillouin zone. This figure shows that good convergence is achieved for the lower 20 bands with the number of plane waves greater or equal to 405. In the case of Fig. 6, where 405 plane waves were taken into account, the worst convergence in reduced frequency is less than 2% of the fully converged FEM eigenfrequency. We also observed an overall agreement between the band structures obtained by Langlet on arrays of cylindrical holes drilled in poly-vinyl-chloride plates applying the finite element method²¹ and that calculated with the SC-PWE method using LIM as the inclusion material. This agreement is achieved with $M_x=M_y=M_z=3$. All our numerical results using the LIM as the inclusion material suggest

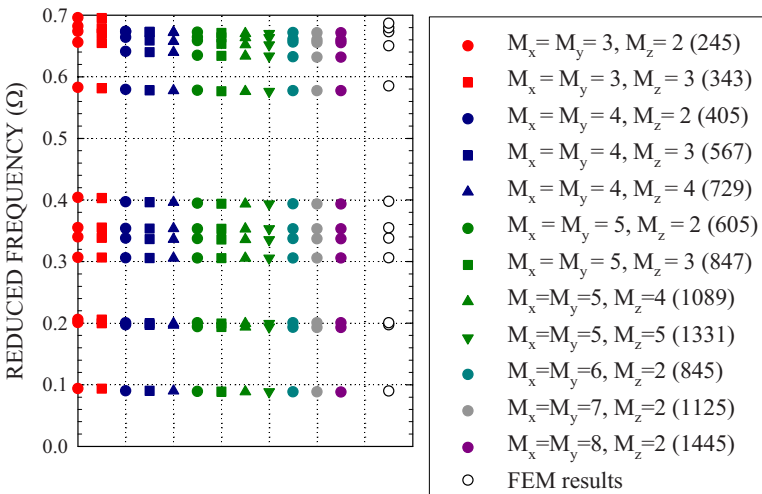


FIG. 7. (Color online) Eigenvalues at the X point of the Brillouin zone calculated with the SC-PWE method as a function of M_x , M_y , and M_z (i.e., the number of plane waves) for the air-steel phononic crystal plate of Fig. 6. The open circles represent the eigenvalues computed with the FE method and serve as a fully converged reference. Note the excellent convergence of the SC-PWE method starting at a relatively small number of plane waves.

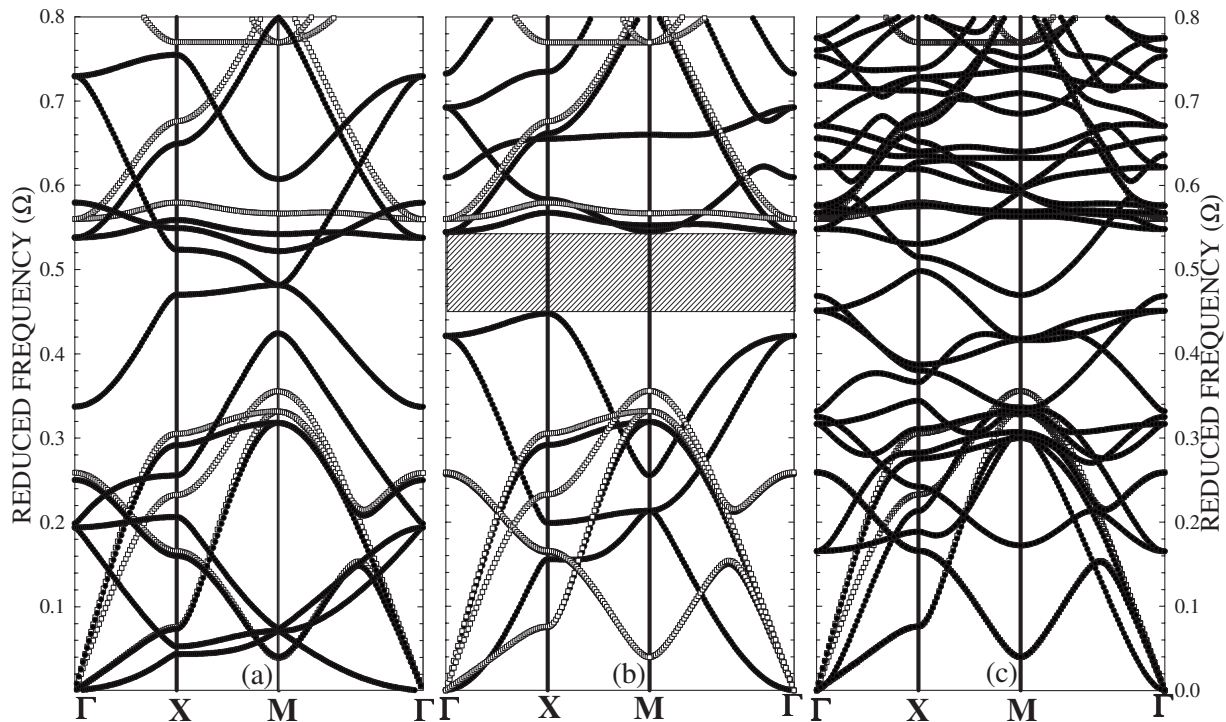


FIG. 8. SC-PWE band structures for the bulk 2D phononic crystal (open squares) and the phononic crystal plate of thickness h_2 (black filled circles) made of a square array of air (LIM) holes embedded in silicon with $f=0.7$. (a) $h_2=0.1a$; (b) $h_2=0.55a$; (c) $h_2=2a$. The dashed area in (b) shows the absolute band gap for the plate. The SC-PWE calculation used $M_x=M_y=4$, $M_z=2$, i.e., 845 plane waves.

that the SC-PWE method provides a mean of calculating the band structure of air-solid 2D phononic crystal plates reliably with a reasonably small number of plane waves in the Fourier series expansion and this over a wide range of matrix material.

2. Air-cubic matrix systems

With a reasonably fast converging SC-PWE method for air-solid systems, we now investigate a 2D phononic crystal plate constituted of a material commonly used in microfabrication, namely, silicon. The first plate is composed of a square array of air holes. Figure 8 reports the elastic band structures of the bulk phononic crystal and of phononic crystal plates with varying thicknesses for a filling factor fixed to 0.7. The plate modes differ significantly from the bulk band structures. The thin ($h_2=0.1a$) and thick plates ($h_2=2a$) of Figs. 8(a) and 8(c) do not exhibit band gap. An absolute band gap occurs in Fig. 8(b) for a plate thickness of $0.55a$. The complete evolution of the gap width with the ratio h_2/a is presented in Fig. 9 showing closing of the gap for thicknesses below $0.2a$ and above $0.9a$. One may search for larger band gaps with the same constituent materials by changing the geometry of the array of inclusions. Indeed, it is well known that bulk phononic crystal geometry plays a fundamental role in designing large elastic band gaps. Subsequently we investigated the dispersion curves of 2D phononic crystal plates with the graphite structure. Figure 10 shows the bulk band structure (hollow squares) and the dispersion curves of a phononic crystal plate (black filled circles) for a graphite array of holes in silicon with $f_1=2$

=0.25, i.e., a total filling factor f of inclusions equals to 0.5, smaller than the close-packing value of 0.604. We consider plates of varying thickness. The characteristic “lattice” parameter of the graphite array is not a but rather $a\sqrt{3}$, i.e., the length of the sides of the 2D primitive unit cell of the graphite array [see Fig. 1(b)]. Then we study the evolution of the band structure of the plate as a function of the ratio between the plate thickness h_2 and $a\sqrt{3}$. As in the previous cases, the band structure of the plate differs from that of the infinite

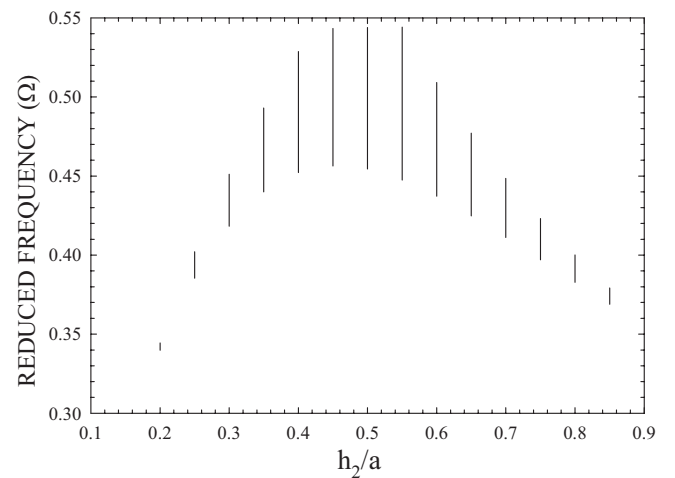


FIG. 9. Location and width of the band gap versus the ratio of the plate thickness h_2 to the lattice parameter a for air-silicon phononic crystal plate with a square array of holes. All other parameters (f, M_x, M_y, M_z) are the same as those of Fig. 8.

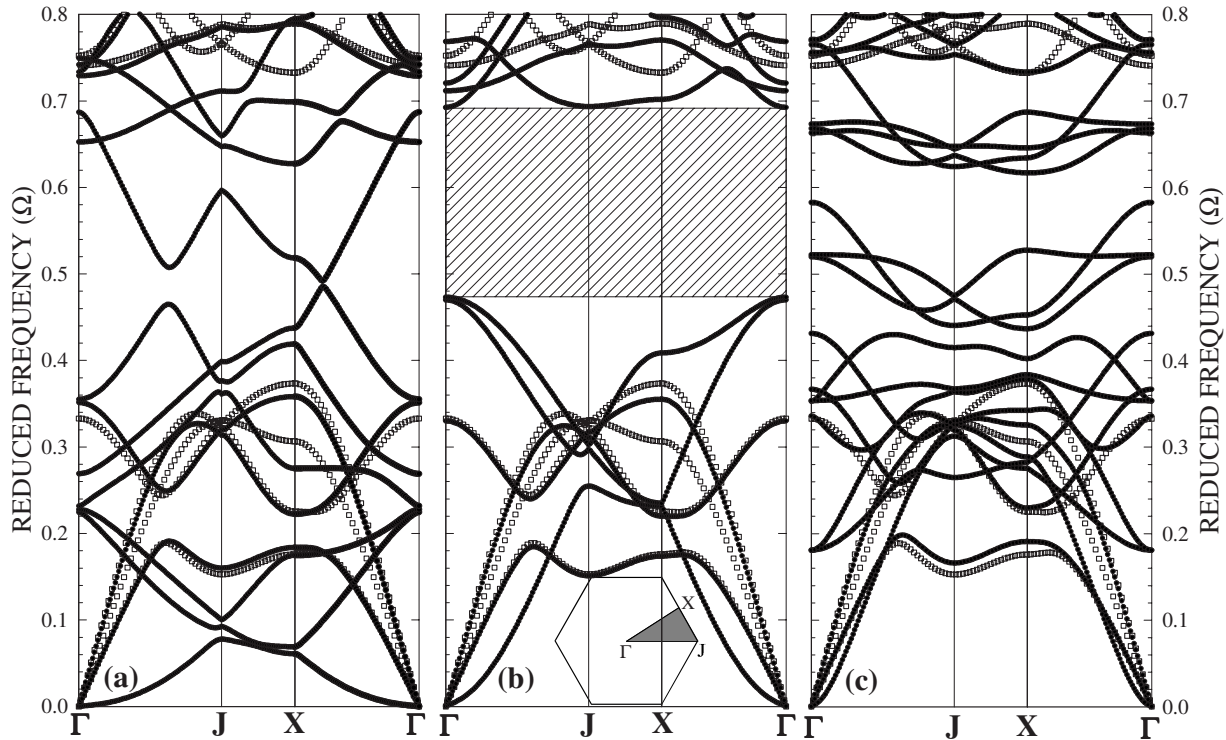


FIG. 10. SC-PWE band structures for the bulk 2D phononic crystal (open squares) and the phononic crystal plate of thickness h_2 (black filled circles) made of a graphite array of air (LIM) holes embedded in silicon with $f=f_1+f_2=0.5$. (a) $\frac{h_2}{a\sqrt{3}}=0.1$; (b) $\frac{h_2}{a\sqrt{3}}=0.58$; (c) $\frac{h_2}{a\sqrt{3}}=2$. The results are rendered in terms of a reduced frequency $\Omega=\omega a\sqrt{3}/2\pi C_t$, versus a reduced wave vector $\vec{k}=\vec{k}a\sqrt{3}/2\pi$ where $C_t=\sqrt{C_{44}/\rho}=\sqrt{C_{44}(\vec{G}=\vec{0})/\rho(\vec{G}=\vec{0})}$ is an average transverse speed of sound. The inset represents the first Brillouin zone ($\Gamma J X$) of the graphite array. The components of the wave vector \vec{k} at the Γ , J , and X points are $\frac{2\pi}{a\sqrt{3}}(0,0)$, $\frac{2\pi}{a\sqrt{3}}(\frac{2}{3},0)$, and $\frac{2\pi}{a\sqrt{3}}(\frac{1}{2},\frac{1}{2\sqrt{3}})$. The SC-PWE calculation used $M_x=M_y=4$, $M_z=2$, i.e., 845 plane waves.

phononic crystal. On the other hand, the width of the full band gap centered around $\Omega \approx 0.6$ in Fig. 10(b) is markedly larger than the gaps reported in the case of the square array. As previously, the existence of this absolute stop band depends on the thickness h_2 of the plate and the optimum value of h_2 is of the order of magnitude of $0.58a\sqrt{3}$. In Fig. 10(c), absolute band gap remains for a thickness of $2a\sqrt{3}$. In Fig. 11, we present the position and width of the first band gap as a function of the ratio $h_2/a\sqrt{3}$. Figure 11 shows that absolute band gap vanishes for $h_2/a\sqrt{3} < 0.2$. For the graphite structure, the band gap does not close before the ratio $h_2/a\sqrt{3}$ exceeds 1.15. One observes that the larger gap appears for $h_2/a\sqrt{3} \approx 0.58$. Then the variation of the gap width with the ratio between the thickness of the plate and the characteristic “lattice” parameter for both square and graphite networks of holes scales in a similar way. Moreover, while for the square array of holes, absolute band gaps were obtained for filling factors approaching the close-packed value for which cylinders are in contact with one another, the graphite network shows wide gaps for noncontacting cylinders. Consequently, the technical realization of phononic crystals made of holes in a solid matrix exhibiting absolute stop bands at very high frequencies is probably much easier when the holes are arranged upon a graphite array than a square network especially at the scale of a thin plate. Moreover, we have verified that the effect of the geometry of the inclusion (square rather

than cylindrical inclusion) in that case of air-solid 2D phononic crystal plate is minimal as already observed in bulk phononic crystals.³

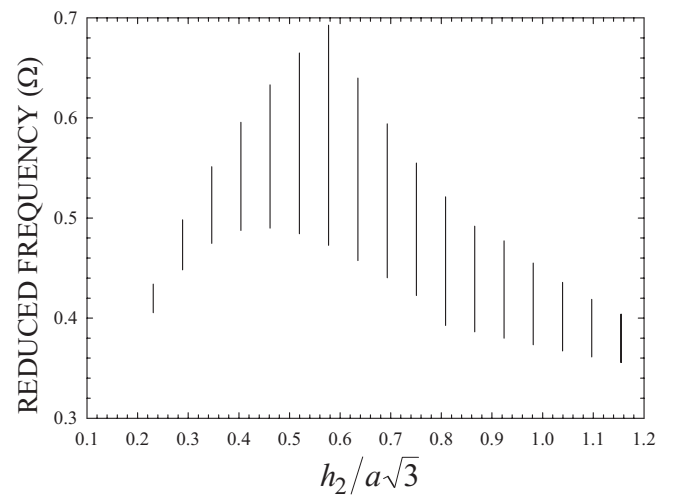


FIG. 11. Location and width of the band gap versus the ratio of the plate thickness h_2 to the characteristic lattice parameter $a\sqrt{3}$ for an air-silicon phononic crystal plate with a graphite array of holes. All other parameters (f, M_z, M_y, M_z) are the same as those of Fig. 10.

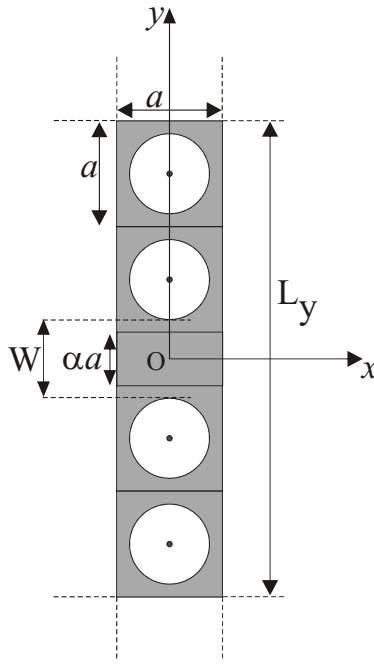


FIG. 12. Schematic illustration of the supercell used for the SC-PWE calculation of the band structure of a defected phononic crystal plate.

C. Waveguide in air-silicon 2D phononic crystal plate

Bulk phononic crystals containing rectilinear defects have been shown to guide elastic waves efficiently.^{5,28–30} Moreover surface acoustic waves can also be guided in defective semi-infinite 2D phononic crystals.³¹ In a very recent paper, Sun and Wu used the finite difference time domain method for investigating the propagation of elastic waves through

waveguides in a 2D phononic crystal plate made of solid constituents.³² In addition to the calculation of band structures of perfect 2D phononic crystal plates, the SC-PWE method can also be extended to study wave propagation in defective plate structures. More specifically, we consider a phononic crystal constituted of a square array of LIM holes in a Si plate with a filling fraction $f=0.7$. Here we extend the SC-PWE method to the calculation of the band structure of 2D phononic crystal plates with a linear defect of variable width. The guide is obtained by removing a row of holes along the x direction and varying the distance between the two neighboring rows of holes. This is done numerically by considering a rectangular supercell of width along the x direction equals to a and a length along the y direction, $L_y > a$. The thickness of the supercell along the z direction remains equal to $\ell=h_1+h_2+h_3$. The structure of the defected supercell is illustrated in Fig. 12. In this figure, aa represents the separation distance between the edges of the two unit cells adjacent to the waveguide. aa is an adjustable geometrical parameter. For $\alpha=0$, the structure is that of a supercell containing N_{cyl} holes arranged on a perfect square lattice, namely a supercell of the perfect phononic crystal plate. If $\alpha=1$ the structure is that of a 2D phononic crystal plate with one row of holes filled with the matrix material. One can vary the width of the waveguide by setting $\alpha \neq 0$. The width W of the guide defined as the closest distance between the surface of the holes on either sides of the guide is given by $W=(1+\alpha)a-2R$. This supercell is repeated periodically in the x , y , and z directions. We choose the thickness h_2 of the slab equals to $0.55a$ for ensuring the existence of the largest gap in the perfect phononic crystal plate. The thicknesses h_1 and h_3 of the LIM slabs are equal to a . Due to the periodicity in the y direction, the expression of the Fourier coefficients defined by Eq. (12) must be modified as

$$\zeta(\vec{G}) = \begin{cases} \zeta_A f \frac{N_{cyl}}{(L_y/a)} \left(\frac{h_2}{\ell} \right) + \zeta_B \left[1 - \frac{N_{cyl}}{(L_y/a)} f \right] \left(\frac{h_2}{\ell} \right) + \zeta_C \left(\frac{h_1}{\ell} \right) + \zeta_D \left(\frac{h_3}{\ell} \right) & \text{if } \vec{G} = \vec{0} \\ (\zeta_A - \zeta_B) \frac{1}{(L_y/a)} \sum_i^{N_{cyl}} e^{-i\vec{G}\cdot\vec{r}_i} F_I^{wg}(\vec{G}) + (\zeta_C - \zeta_B) F_H^{wg}(\vec{G}) + (\zeta_D - \zeta_B) F_{II}^{wg}(\vec{G}) & \text{if } \vec{G} \neq \vec{0}, \end{cases} \quad (17)$$

with

$$\begin{aligned} F_I^{wg}(\vec{G}) &= \frac{1}{V_u} \int \int \int_{(A)} e^{-i\vec{G}\cdot\vec{r}} d^3\vec{r} \\ &= F(\vec{G}_{||}) \left[\frac{\sin\left(G_z \frac{h_2}{2}\right)}{\left(G_z \frac{h_2}{2}\right)} \right] \left(\frac{h_2}{\ell} \right), \end{aligned} \quad (18a)$$

$$\begin{aligned} F_{II}^{wg}(\vec{G}) &= \frac{1}{V_u} \int \int \int_{(C)} e^{-i\vec{G}\cdot\vec{r}} d^3\vec{r} = \left[\frac{\sin\left(G_x \frac{a}{2}\right)}{\left(G_x \frac{a}{2}\right)} \right] \\ &\times \left[\frac{\sin\left(G_y \frac{L_y}{2}\right)}{\left(G_y \frac{L_y}{2}\right)} \right] \left[\frac{\sin\left(G_z \frac{h_1}{2}\right)}{\left(G_z \frac{h_1}{2}\right)} \right] \left(\frac{h_1}{\ell} \right) e^{-iG_z[(h_1+h_2)2]}, \end{aligned} \quad (18b)$$

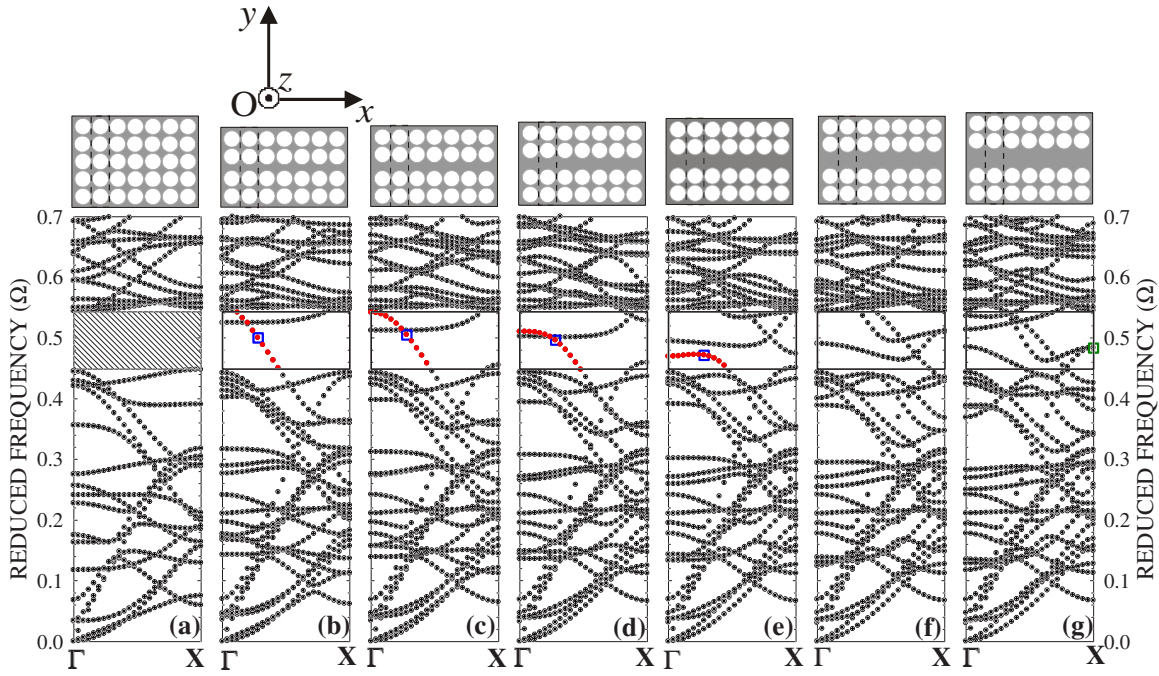


FIG. 13. (Color online) Band structures along the Γ X direction of (a) the perfect phononic crystal plate ($\alpha=0$ and $N_{\text{cyl}}=5$), (b) the phononic crystal plate containing a waveguide with $\alpha=0.25$ and $N_{\text{cyl}}=4$, (c) the same as in (b) but with $\alpha=0.4$, (d) the same as in (b) but with $\alpha=0.55$, (e) the same as in (b) but with $\alpha=0.7$, (f) the same as in (b) but with $\alpha=0.85$, and (g) the same as in (b) but with $\alpha=1.0$. αa represents the separation distance between the edges of the two unit cells adjacent to the waveguide. The SC-PWE calculation used $M_x=4$, $M_y \cdot M'_y = 4 \cdot 5 = 20$, $M_z=2$, i.e., 1845 plane waves. The dashed area in (a) shows the absolute band gap for the plate. In (b), (c), (d), and (e) [(g)], the blue (green) square indicates the location of the guided modes analyzed in Fig. 14 (Fig. 15).

$$F_{III}^{wg}(\vec{G}) = \frac{1}{V_u} \int \int \int_{(D)} e^{-i\vec{G} \cdot \vec{r}} d^3 \vec{r} = \left[\frac{\sin\left(G_x \frac{a}{2}\right)}{\left(G_x \frac{a}{2}\right)} \right] \times \left[\frac{\sin\left(G_y \frac{L_y}{2}\right)}{\left(G_y \frac{L_y}{2}\right)} \right] \left[\frac{\sin\left(G_z \frac{h_3}{2}\right)}{\left(G_z \frac{h_3}{2}\right)} \right] \left(\frac{h_3}{\ell} \right) e^{-iG_z[(h_2+h_3)/2]} \quad (18c)$$

In order to follow the evolution of the dispersion curves of the defective phononic crystal plate as a function of the waveguide width, we have investigated seven systems. The first system corresponds to a perfect phononic crystal plate with a supercell containing $N_{\text{cyl}}=5$ with $\alpha=0$. For the seventh system, we have chosen $\alpha=1$ and $N_{\text{cyl}}=4$. This structure is equivalent to filling with silicon, one of the five holes in the first system effectively resulting in a linear defect along the x direction. The other systems with $N_{\text{cyl}}=4$ and α ranging from 0.25 to 0.85 by step of 0.15 are similar to the seventh system but with a narrower waveguide. Because of the periodicity, the waveguide is repeated in the y direction leading to a stack of waveguides separated by four air holes. This separation is sufficient to avoid significant coupling between neighboring guides.

The band structures, computed along the Γ X direction (i.e., the direction of propagation of a wave along the linear waveguide) of the seven systems, are reported in Fig. 13.

Since the supercell is longer in the y direction, a larger number of reciprocal vectors is required along the y direction for satisfactory convergence. $(2M_x+1)(2M_y \cdot M'_y+1)(2M_z+1)=1845$ (with $M_x=M_y=4$, $M_z=2$, and $M'_y=5$) reciprocal lattice vectors were taken into account for computing these dispersion curves. Figure 13(a) exhibits numerous additional branches than that of Fig. 8(b) (i.e., the band structure calculated with a single unit cell along the y direction) as the result of the folding of the bands in the y direction due to the five unit cell periodicity in that direction. This system still shows the forbidden band. Formation of a waveguide in that structure inserts guided modes inside the band gap of the perfect phononic crystal as illustrated in Figs. 13(b)–13(g). Figure 13 shows that when the width of the waveguide increases, the number of guided modes in the band gap increases. This is the standard behavior observed in waveguide theory. One considers now a specific waveguide mode that falls inside the band gap of the perfect phononic crystal plate. This mode is represented with red dots in Figs. 13(b)–13(e). One observes that the location of this mode inside the stop band of the perfect phononic crystal plate depends strongly on the width of the waveguide. This mode evolves from a location near the top of the gap to near the bottom of the gap as the width of the waveguide increases. This mode merges with the passband below the band gap for α larger than 0.7. We characterize this guided mode further by calculating the modulus of the complex components of the displacement field for different values of α . For example, Fig. 14 shows the maps of the modulus of these components for this specific mode for a fixed value of the wave vector, i.e., $K_x=0.14(2\pi/a)$ [blue square in Figs. 13(b)–13(e)]. Fig-

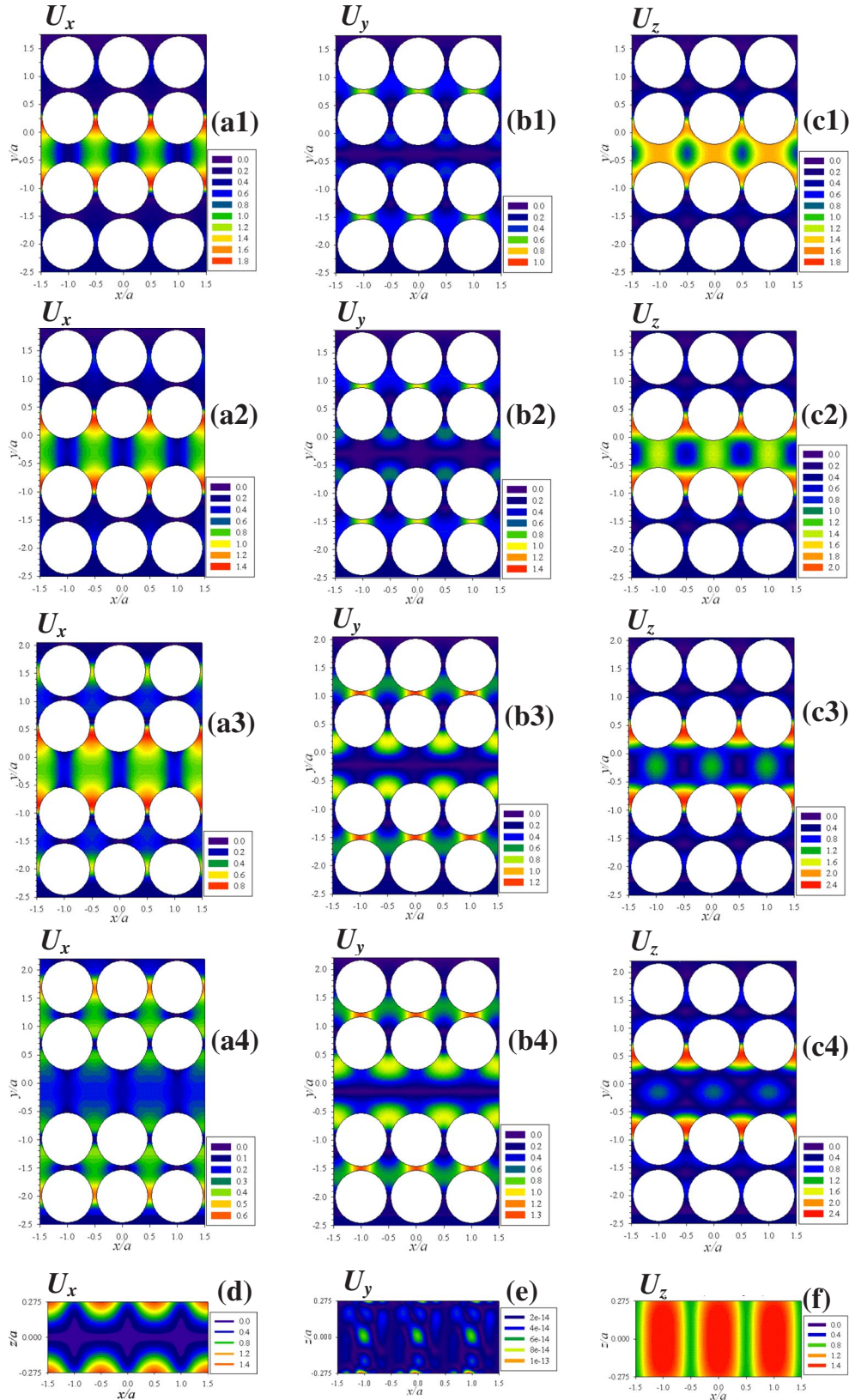


FIG. 14. (Color online) Maps of the modulus (in arbitrary units) of the complex components of the elastic displacement field in (a1), (b1), (c1) the xOy ($z=0.2a$) plane and (d), (e), (f) the xOz plane at the center of the waveguide for the waveguide mode with $\Omega=0.5001$ at the $K_x=0.14$, $(\frac{2\pi}{a})$ point for the narrowest waveguide [see blue square in Fig. 13(b)]. (a2), (b2), and (c2): the same as in (a1), (b1), and (c1) but for the mode represented with a blue square in Fig. 13(c); (a3), (b3), and (c3): the same as in (a1), (b1), and (c1) but for the mode represented with a blue square in Fig. 13(d); (a4), (b4), and (c4): the same as in (a1), (b1), and (c1) but for the mode represented with a blue square in Fig. 13(e).

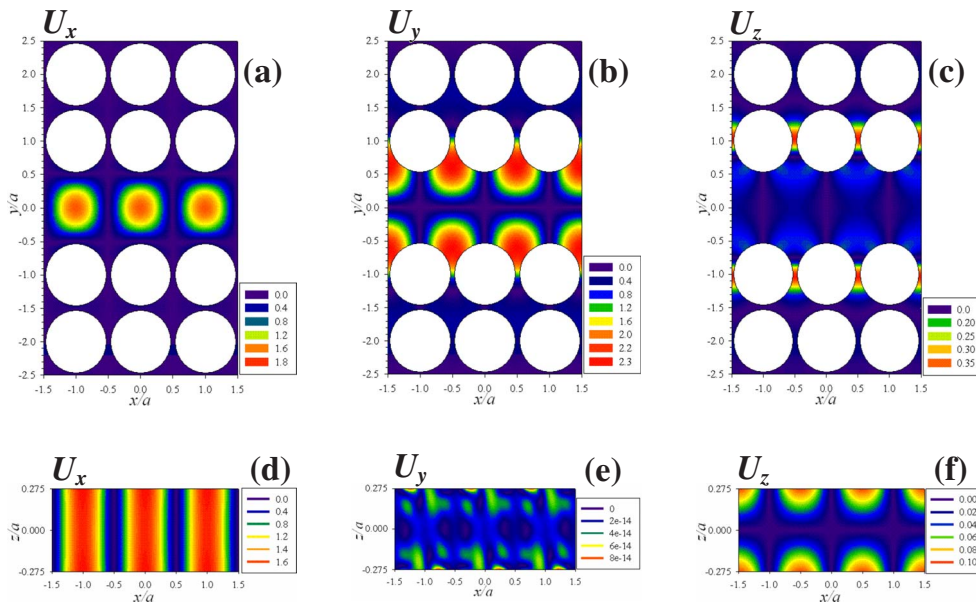


FIG. 15. (Color online) Maps of the modulus (in arbitrary units) of the complex components of the elastic displacement field in (a), (b), (c) the xOy ($z=0.2a$) plane and (d), (e), (f) the xOz plane at the center of the waveguide for the waveguide mode with $\Omega=0.4834$ at the X point for the widest waveguide [see green square in Fig. 13(g)].

ures 14(a1)–14(c4) correspond to cuts of the three-dimensional displacement field in the (xOy) plane at a position $z=0.2a$, which is near the top surface of the plate. One observes that for $\alpha=0.25$, the guided mode which appears approximately at the center of the stop band [see Fig. 13(b)] is confined within or in the close vicinity of the waveguide (see top panel of Fig. 14). The displacement field penetrates the interspace between the adjacent cylinders but becomes negligible once one leaves the close vicinity of the guide.³³ For a larger waveguide, while the z component of this mode remains well confined into the waveguide, the other components leak out into the phononic crystal structure. The mode becomes less and less confined to the waveguide as the width of the waveguide increases. In Figs. 13(c) and 13(d), one notes that the mode we consider crosses another mode for this value of K_x . These two modes may interact strongly together and this has probably a detrimental effect on the waveguide mode confinement. For $\alpha=0.7$, the mode is very close to the bottom of the stop band [see Fig. 13(e)] and this may explain the very weak confinement of the mode. The bottom panel of Fig. 14 shows cuts of the displacement field in the (xOz) plane located at a position along the y direction corresponding to the center of the guide for the waveguide mode considered in Fig. 13(b) for $\alpha=0.25$ and $K_x=0.14\cdot(2\pi/a)$. We use these figures to define the polarization of the mode in the (xOz) plane. At the center of the waveguide, due to the symmetry of the mode, the y component of the displacement field is negligible while the x component is fairly localized near the surfaces of the plate. The z component varies slowly along the x direction. We checked that the modes depicted by a blue square in Figs. 13(b)–13(e) possess the same polarization in the (xOz) plane than that described in the bottom panel of Fig. 14. Figure 15 presents the maps of the displacement field for the waveguide mode with $\Omega=0.4834$ at the X point for the wider guide. This mode

is represented with a green square in Fig. 13(g). In this case, the wave vector corresponds to one of the highest symmetry point in the square Brillouin zone. Notes that at this \vec{K} point another mode appears at a slightly higher reduced frequency, i.e., $\Omega=0.4836$. One observes in the top panel of Fig. 15 that the confinement of the waveguide mode with $\Omega=0.4834$ is very good in this large waveguide and does not suffer from the possible interaction between these two modes. The bottom panel of Fig. 15 shows that in that case, the z component of the displacement field is localized to the vicinity of the surfaces of the plate. The polarization of this mode differs from that depicted in Figs. 14(d)–14(f) for the guided mode of the narrowest waveguide. A comparison between the bottom panels of Figs. 14 and 15 indicates that depending upon the polarization of the mode, the x or z component of the displacement field of the guided mode may be localized on the surfaces of the plate. Moreover the thickness of the plate governs the width of the absolute band gap of the perfect phononic crystal plate. As observed in these results (see Figs. 14 and 15) and also in the case of guided modes in bulk phononic crystals,³³ a guided mode is confined more effectively inside the waveguide if it appears in the band structure far away from the edges of the stop band. One may suppose that due to the narrower stop band, a guided mode will be less confined inside the waveguide when considering a thinner or thicker phononic crystal plate.

IV. CONCLUSION

We introduce a supercell plane wave expansion method to calculate the elastic band structures of perfect and defected 2D phononic crystal plates. Compared with previous works on waves propagating in 2D phononic crystals with free surfaces, our method does not require writing explicitly the boundary conditions on the free surfaces. This alleviates

some numerical difficulties such as the computation of pseudomodes without physical meaning.^{7,8,12} We establish the range of validity of this method with respect to the contrast in material properties and phononic crystal plate geometry. We demonstrate for solid-solid phononic crystals with low contrast materials that the method converges with a reasonably small number of reciprocal space vectors in all directions. High contrast solid-solid phononic crystal plates have been shown to lead to convergence difficulties for most of the PWE-based methods introduced to date. The SC-PWE method suffers the same problem. We propose a low impedance medium (LIM) to serve as decoupling medium between periodically repeated plates. We also show that the LIM can be used effectively as an inclusion medium to model 2D phononic crystal plates composed of air inclusions and solid matrices. We establish that this approach leads to fast convergence for a wide range of values of solid physical properties. We show the existence of band gaps in air-steel and air-silicon 2D phononic crystal plates composed of square arrays of holes. We also observe wider band gaps for a graphite lattice of air holes in silicon plates. We characterize the effect of the thickness of the plate on the location and the width of the absolute band gaps and find optimum conditions

for achieving the widest absolute band gap. Finally, we apply the SC-PWE method with LIM inclusions to a study of air-silicon phononic crystal plates containing a guide of variable width. The defected system is composed of two phononic crystal plates separated by a homogeneous solid plate made of silicon. We demonstrate the existence of waveguide modes inside the absolute forbidden bands. The number of waveguide modes decreases with a decreasing width of the guide. Characterization of the displacement fields associated with the waveguide modes demonstrates, in some cases, their localization inside this structural defect. These defect modes could then be used to realize acoustic devices such as waveguides, specific frequency filters, or wavelength demultiplexers. In particular, these functionalities are of interest in radio-frequency devices for telecommunication applications.³⁴

ACKNOWLEDGMENTS

This work was supported by “Le Fond Européen de Développement Régional” and “Le Conseil Régional Nord-Pas de Calais.” P.A.D. would like to thank the University of Lille I for its hospitality.

*Author to whom correspondence should be addressed.
jerome.vasseur@univ-lille1.fr

¹J. O. Vasseur, B. Djafari-Rouhani, L. Dobrzynski, M. S. Kushwaha, and P. Halevi, *J. Phys.: Condens. Matter* **6**, 8759 (1994).

²M. M. Sigalas and E. N. Economou, *Solid State Commun.* **86**, 141 (1993).

³I. Sliwa and M. Krawczyk, *Acta Phys. Pol. A* **108**, 943 (2005).

⁴J. O. Vasseur, B. Djafari-Rouhani, L. Dobrzynski, and P. A. Deymier, *J. Phys.: Condens. Matter* **9**, 7327 (1997).

⁵Y. Pennec, B. Djafari-Rouhani, J. O. Vasseur, A. Khelif, and P. A. Deymier, *Phys. Rev. E* **69**, 046608 (2004).

⁶Y. Pennec, B. Djafari-Rouhani, J. O. Vasseur, H. Larabi, A. Khelif, A. Choujaa, S. Benchabane, and V. Laude, *Appl. Phys. Lett.* **87**, 261912 (2005).

⁷Y. Tanaka and S. I. Tamura, *Phys. Rev. B* **58**, 7958 (1998).

⁸Y. Tanaka and S. I. Tamura, *Phys. Rev. B* **60**, 13294 (1999).

⁹T. T. Wu, Z. G. Huang, and S. Lin, *Phys. Rev. B* **69**, 094301 (2004).

¹⁰V. Laude, M. Wilms, S. Benchabane, and A. Khelif, *Phys. Rev. E* **71**, 036607 (2005).

¹¹J. J. Chen, B. Qin, and J. C. Cheng, *Chin. Phys. Lett.* **22**, 1706 (2005).

¹²C. Charles, B. Bonello, and F. Ganot, *Ultrasonics* **44**, 1209(E) (2006).

¹³J. C. Hsu and T. T. Wu, *Phys. Rev. B* **74**, 144303 (2006).

¹⁴B. Manzanares-Martinez and F. Ramos-Mendieta, *Phys. Rev. B* **68**, 134303 (2003).

¹⁵R. Sainidou and N. Stefanou, *Phys. Rev. B* **73**, 184301 (2006).

¹⁶T. T. Wu, Z. G. Huang, and S. Y. Liu, *Z. Kristallogr.* **220**, 841 (2005); T. T. Wu, L. C. Wu, and Z. G. Huang, *J. Appl. Phys.* **97**, 094916 (2005).

¹⁷S. Benchabane, A. Khelif, J.-Y. Rauch, L. Robert, and V. Laude, *Phys. Rev. E* **73**, 065601(R) (2006).

¹⁸X. Zhang, T. Jackson, E. Lafond, P. Deymier, and J. O. Vasseur, *Appl. Phys. Lett.* **88**, 041911 (2006).

¹⁹C. Goffaux and J. P. Vigneron, *Phys. Rev. B* **64**, 075118 (2001).

²⁰Y. Tanaka, Y. Tomoyasu, and S. I. Tamura, *Phys. Rev. B* **62**, 7387 (2000).

²¹Ph. Langlet, Ph.D thesis, Université de Valenciennes et du Hainaut-Cambrésis, 1993.

²²The band structures were computed with the help of the ATILA finite element code; ATILA finite element code for piezoelectric and magnetostrictive transducers modeling, Version 5.2.1, User’s Manual, ISEN, Acoustics Laboratory, Lille, France, 2002.

²³Ph. Langlet, A.-C. Hladky-Hennion, and J.-N. Decarpigny, *J. Acoust. Soc. Am.* **98**, 2792 (1995).

²⁴A. Khelif, B. Aoubiza, S. Mohammadi, A. Adibi, and V. Laude, *Phys. Rev. E* **74**, 046610 (2006).

²⁵J. O. Vasseur, P. A. Deymier, B. Chenni, B. Djafari-Rouhani, L. Dobrzynski, and D. Prevost, *Phys. Rev. Lett.* **86**, 3012 (2001).

²⁶T. Gorishnyy, C. K. Ullal, M. Maldovan, G. Fytas, and E. L. Thomas, *Phys. Rev. Lett.* **94**, 115501 (2005).

²⁷M. Maldovan and E. L. Thomas, *Appl. Phys. B: Lasers Opt.* **83**, 595 (2006).

²⁸A. Khelif, A. Choujaa, S. Benchabane, B. Djafari-Rouhani, and V. Laude, *Z. Kristallogr.* **220**, 836 (2005).

²⁹T. Miyashita and C. Inoue, *Jpn. J. Appl. Phys., Part 1* **40**, 3488 (2001).

³⁰T. Miyashita, *Meas. Sci. Technol.* **16**, R47 (2005).

³¹J.-H. Sun and T. T. Wu, *Phys. Rev. B* **74**, 174305 (2006).

³²J.-H. Sun and T. T. Wu, *Phys. Rev. B* **76**, 104304 (2007).

³³J. O. Vasseur, P. A. Deymier, M. Beaugeois, Y. Pennec, B. Djafari-Rouhani, and D. Prevost, *Z. Kristallogr.* **220**, 829 (2005).

³⁴C. Campbell, *Surface Acoustic Wave Devices for Mobile and Wireless Communications* (Academic, San Diego, CA, 1985).